

Review of Wu et al., "Evaluation of autoconversion and accretion enhancement factors in GCM warm-rain parameterizations using ground-based measurements at the Azores," first revision

I must start by acknowledging the major effort undertaken by the authors to address my comments on the initial submission, especially with respect to obtaining collocated, vertically-resolved cloud and rain liquid water contents. I'm sure this was a significant undertaking, but it puts the premise of their analysis on solid footing and gives me much greater confidence in their conclusions. The addition of Appendix A to demonstrate the rain water content retrieval is also greatly appreciated. I still have a number of minor comments and there remain many language issues that introduce ambiguity in interpreting the authors' statements. I therefore recommend **acceptance pending minor revisions** to address these comments, and I **strongly** recommend the authors use a professional copyediting service to handle the language issues.

Other general comments:

- It's misleading that you call the effective length scale calculated from (wind speed * time elapsed) a "model grid size." It would be more accurate to use language such as "equivalent grid size" or "equivalent model grid size."
- There is a pervasive units issue. Almost everywhere that grid size is given as an area, the units are given in km where they should be km². Please correct throughout the manuscript or change all instances to "horizontal grid size of X km" such that they do not reference an area.
- Using a constant value of DSD width is analogous to using a constant LWC distribution width or $E_{\text{auto}}/E_{\text{accr}}$ width – the spectral width of the DSD is something that varies (increases) with length scale (e.g. Geoffroy et al, 2010, ACP) and is also dependent on the choice of in situ instrumentation (e.g. Witte et al., 2018, GRL; also mentioned but not dealt with in Miles et al., 2000, JAS). While I don't think there's an obvious "better" solution at this point (the math would get considerably hairier if one also considers variable DSD shape), I think it's important to note that by making this assumption, you're essentially just kicking the use of "parameters constant with length scale" down the line from LWC distributions to DSD width. This seems particularly prescient given that your argument for regime-dependence is reflected in the finding of Miles et al. (2000) that the distribution of DSD parameters is different for marine and continental clouds.

Specific content-related comments are given in the remainder of the review in reference to page and line number(s) (format: PX, LY-Z = page X, lines Y-Z). Please see

the annotated PDF following these comments for a non-comprehensive list of language issues.

P1, L33: This sentence gives the impression that there is a particular value that the q_r - q_c ratio *should* be. Be more explicit here about why this value matters – just throwing out the values without context (e.g. observed vs. typical GCM values) doesn't "prove" that the presently-used constant enhancement factors are wrong.

P3, L55: How do aerosol effects being tied to precipitation suppression fit with the rest of your argument? I fail to see the relevance, especially since your results show that precipitation frequency has almost no relationship with E_{auto,N_c} .

P4, L60-62: I don't see the point of this sentence. If you're getting at the idea that the "cloud" and "rain" sub-categories are an arbitrary division by drop size, say so.

P4, L72: Is there not one single study that parameterizes accretion as something other than a power law? You're on firmer ground saying "The vast majority" or something like that because it only takes one counterexample to make your statement false.

P5, L91-93: Cheng and Xu's autoconversion equation is independent of vertical velocity and rain mixing ratio (Text in right column of pg 2319 and their Eq. 6).

P6, L 109: Why is recognition of spatial scales the important aspect? This seems trivial. Please expand.

P6, L113-114: Do you mean Zhang et al. derived sub-grid distributions or the actual pixel-scale CLWP and N_c ? Please clarify.

P7, L131-132: Enhancement factors are applied at the grid scale by definition, so it seems repetitive to say "grid-mean process enhancement factors."

P15, L268: You don't show q_r in Fig 1. Either reference rain LWC as shown in Fig. A1 or remove "and q_r " from the sentence.

P17, L305: What does "relative constant" mean? Clarify what the adjective means or remove it.

P18, L317-319: There are a number of other explanations for this result: the dependence of autoconversion parameterizations on number concentration may be flawed, there could be problems with your number concentration retrieval, or perhaps the assumption of constant N_c with height doesn't work. Unless you have evidence

that a) there is significant subgrid variability of N_c and b) it matters at the process level, I don't think you can make this statement.

P22, L402-404: The differences from prescribed values only have explanatory power if the simulations used to diagnose it were run at something comparable to 30 km horizontal resolution. Do you have a reference to support this?

P22, L410: The language "...the location we choose to collect ground-based observations..." implies that the authors were the primary decision makers regarding the location of the CAP-MBL deployment. If this is the case, this wording is fine. Otherwise, considering alternate wording, e.g. "...the location of the ground-based observations and retrievals used in this study is..."

P25, L464: Use the 180^2 km^2 value here for consistency. You use 120^2 km^2 here while you show a maximum grid size of 180^2 km^2 in the figures and use this same maximum grid size in reference to E_{accr} below.

P28, L519-520: This sentence is confusing. I think you're trying to say "if the vertical gradient of N_w is negative below cloud base" - can you confirm?

P29, L526-527: Italicize all instances in the text of Z (Z_c , Z_d , etc.). Also, does the subscript "d" indicate drizzle? You use the subscript "r" in Eq. A1 and elsewhere in the main manuscript.

P29, L530: Rearrange Eq. A2 for the value you're actually solving for ($CLWC(1)_{\text{reflectivity}}$).

P29, L536: Eq. A2 only gives reflectivity at cloud base. How do you integrate up for the profile?

P30, L543-544: What if there is no drizzle at cloud top? How good is the assumption that you can just decrease N_w until your criteria is satisfied?

Table 2 (P 42, L819): While visually repetitive, the table is more readable if the upper left corner cell is clear. The entries in the leftmost column should then read (from top to bottom): $LTS > 18 \text{ K}$, $13.5 < LTS < 18 \text{ K}$, $LTS < 13.5 \text{ K}$. You may also consider placing a vertical line between the first and second columns to differentiate between the category column and results/data.

Figure 1, panel c (P44, L825): Why does the histogram look so much different than the fitted gamma distribution? Assuming 5-10 m/s wind speeds there would be something

like 60-120 samples for an equivalent 60 km scale, so is this just a consequence of coarse binning?

Figure 1 caption (P44, L 832): Replace “mean- q_c ” with an overbar over q_c .

Figure 2, panels e-f (P45, L 839): The label “cov(q_c , q_r)” is misleading because you don’t actually show the covariance anywhere.

Figure 2, panels e-f (P45, L839): Consider adding minor ticks to the y axes or plot the ratios on a separate right axis. It’s very difficult to get a sense for the maximum magnitude of q_r/q_c because it’s all below the 0.2 tick.

Figure 2 (P45, L839): Add labels to the y axes to show that both the PDF and (precip frequency/ q_r - q_c ratio) are shown on the same scale, i.e. label y axes “PDF, precipitation frequency” and “PDF, q_r - q_c ratio” or similar. This information shouldn’t be buried at the bottom of the caption.

Figure 5 (P48, L856): How do these adjustments compare with retrieval uncertainty? I ask because you show in Fig. 4 that uncertainty in E decrease with equivalent grid size. For example, if the retrieval uncertainty at 30 km is 20%, then does a q_c adjustment tell you something physical or is it just another way of describing uncertainty?

1 **Evaluation of autoconversion and accretion enhancement factors in GCM warm-rain**
2 **parameterizations using ground-based measurements at the Azores**

3 Peng Wu¹, *Baiké Xi¹, Xiquan Dong¹, and Zhibo Zhang²

4¹ Department of Hydrology and Atmospheric Sciences, The University of Arizona, Tucson,
5 Arizona, USA

6² Physics Department, The University of Maryland, Baltimore County, Maryland, USA

7

8

9 Submitted to Atmospheric Chemistry and Physics (September 17, 2018)

10

11

12 **Keywords:** MBL clouds, enhancement factors, autoconversion and accretion parameterizations

13

14

15

16

17

18* Corresponding author address: Dr. Baiké Xi, Department of Hydrology and Atmospheric
19 Sciences, University of Arizona, 1133 E. James E. Rogers Way, Tucson, AZ 85721-0011.
20 baikexi@email.arizona.edu; Phone: 520-626-8945

21 **Abstract**

22 A great challenge in climate modelling is how to parametrize sub-grid cloud processes, such
23 as autoconversion and accretion in warm rain formation. In this study, we use ground-based
24 observations and retrievals over the Azores to investigate the so-called enhancement factors,
25 E_{auto} and E_{accr} , which are often used in climate models to account for the influences of sub-grid
26 variances of cloud and precipitation water on the autoconversion and accretion processes. E_{auto}
27 and E_{accr} are computed for different model resolutions. The calculated E_{auto} values increases
28 from 1.96 (30 km) to 3.15 (120 km), and the calculated E_{accr} values increase from 1.53 (30 km)
29 to 1.76 (180 km). Comparing the prescribed enhancement factors in Morrison and Gettleman
30 (2008, MG08) to the observed ones, we found that a higher E_{auto} (3.2) at small grids and lower
31 E_{accr} (1.07) are used in MG08, which helps to explain why most of the GCMs produce too
32 frequent precipitation events but with too light precipitation intensity. The ratios of rain to
33 cloud water mixing ratio at $E_{accr}=1.07$ and $E_{accr}=2.0$ are 0.063 and 0.142, respectively, further
34 proving that the prescribed value of $E_{accr}=1.07$ used in MG08 is too small to simulate correct
35 precipitation intensity. Both E_{auto} and E_{accr} increase when the boundary layer becomes less
36 stable, and the values are larger in precipitating clouds ($CLWP > 75 \text{ gm}^{-2}$) than those in
37 nonprecipitating clouds ($CLWP < 75 \text{ gm}^{-2}$). Therefore, the selection of E_{auto} and E_{accr} values in
38 GCMs should be regime-dependent.

39

40 **1. Introduction**

41 Due to their vast areal coverage (Warren et al., 1986, 1988; Hahn and Warren, 2007) and
42 strong radiative cooling effect (Hartmann et al., 1992; Chen et al., 2000), small changes in the
43 coverage or thickness of marine boundary layer (MBL) clouds could change the radiative
44 energy budget significantly (Hartmann and Short, 1980; Randall et al., 1984) or even offset the
45 radiative effects produced by increasing greenhouse gases (Slingo, 1990). The lifetime of MBL
46 clouds remains an issue in climate models (Yoo and Li, 2012; Jiang et al., 2012; Yoo et al.,
47 2013; Stanfield et al., 2014) and represents one of the largest uncertainties in predicting future
48 climate (Wielicki et al., 1995; Houghton et al., 2001; Bony and Dufresne, 2005).

49 MBL clouds frequently produce precipitation, mostly in the form of drizzle (Austin et al.,
50 1995; Wood, 2005a; Leon et al., 2008; Wood, 2012). A significant amount of drizzle is
51 evaporated before reaching the surface, for example, about ~76% over the Azores region in
52 Northeast Atlantic (Wu et al., 2015), which provides another water vapour source for MBL
53 clouds. Due to their pristine environment and their close vicinity to the surface, MBL clouds
54 are especially sensitive to aerosol perturbations (Quaas et al., 2009; Kooperman et al., 2012).
55 **Most aerosol indirect effects are associated with precipitation suppression** (Albrecht, 1989;
56 Ackerman et al., 2004; Lohmann and Feichter, 2005; Wood, 2007). Thus, accurate prediction
57 of precipitation is essential in simulating the global energy budget and in constraining aerosol
58 indirect effects in climate projections.

59 Due to the coarse spatial resolutions of the general circulation model (GCM) grid, many
60 cloud processes cannot be adequately resolved and must be parameterized. For example, warm
61 rain parameterizations in most GCMs treat the condensed water as either cloud or rain from the
62 collision-coalescence process, which is partitioned into autoconversion and accretion sub-
63 processes in model parameterizations (Kessler, 1969; Tripoli and Cotton, 1980; Beheng, 1994;
64 Khairoutdinov and Kogan, 2000; Liu and Daum, 2004). Autoconversion represents the process
65 that drizzle drops being formed through the condensation of cloud droplets and accretion
66 represents the process where rain drops grow by the coalescence of drizzle-sized drops with
67 cloud droplets. Autoconversion mainly accounts for precipitation initiation while accretion
68 primarily contributes to precipitation intensity. Autoconversion is often parameterized as
69 functions of cloud droplet number concentration (N_c) and cloud water mixing ratio (q_c), while
70 accretion depends on both cloud and rain water mixing ratios (q_c and q_r) (Kessler, 1969; Tripoli
71 and Cotton, 1980; Beheng, 1994; Khairoutdinov and Kogan, 2000; Liu and Daum, 2004;
72 Wood, 2005b). All previous studies suggested that these two processes as power law functions
73 of cloud and precipitation properties (See section 2 for details).

74 In conventional GCMs, the lack of information on the sub-grid variances of cloud and
75 precipitation leads to the unavoidable use of the grid-mean quantities ($\overline{N_c}$, $\overline{q_c}$, and $\overline{q_r}$, where
76 overbar denotes grid mean, same below) in calculating autoconversion and accretion rates.
77 MBL cloud liquid water path (CLWP) distributions are often positive skewed (Wood and

78 Hartmann, 2006; Dong et al., 2014a and 2014b), that is, the mean value is greater than mode
79 value. Thus, the mean value only represents a relatively small portion of samples. Also, due to
80 the nonlinear nature of the relationships, the two processes depend significantly on the sub-
81 grid variability and co-variability of cloud and precipitation microphysical properties (Weber
82 and Quass, 2012; Boutle et al., 2014). In some GCMs, sub-grid scale variability is often ignored
83 or hard coded using constants to represent the variabilities under all meteorological conditions
84 and across the entire globe (Pincus and Klein, 2000; Morrison and Gettleman, 2008; Lebsock
85 et al., 2013). This could lead to systematic errors in precipitation rate simulations (Wood et al.,
86 2002; Larson et al., 2011; Lebsock et al., 2013; Boutle et al., 2014; Song et al., 2018), where
87 GCMs are found to produce too frequent but too light precipitation compared to observations
88 (Zhang et al., 2002; Jess, 2010; Stephens et al., 2010; Nam and Quaas, 2012; Song et al., 2018).
89 The bias is found to be smaller by using a probability density function (PDF) of cloud water to
90 represent the sub-grid scale variability in autoconversion parameterization (Beheng, 1994;
91 Zhang et al., 2002; Jess, 2010), or more complexly, by integrating the autoconversion rate over
92 a joint PDF of liquid water potential temperature, vertical velocity, total water mixing ratio and
93 rain water mixing ratio (Cheng and Xu, 2009).

94 Process rate enhancement factors (E) are introduced when considering sub-grid scale
95 variability in parameterizing grid-mean processes and they should be parameterized as
96 functions of the PDFs of cloud and precipitation properties within a grid box (Morrison and

97 Gettleman, 2008; Lebsock et al., 2013; Boutle et al., 2014). However, these values in some
98 GCM parameterization schemes are prescribed as constants regardless of underlying surface
99 or meteorological conditions (Xie and Zhang, 2015). Boutle et al. (2014) used aircraft in situ
100 measurements and remote sensing techniques to develop a parameterization for cloud and rain,
101 in which not only consider the sub-grid variabilities under different grid scales, but also
102 consider the variation of cloud and rain fractions. The parameterization was found to reduce
103 precipitation estimation bias significantly. Hill et al. (2015) modified this parameterization and
104 developed a regime and cloud type dependent sub-grid parameterization, which was
105 implemented to the Met Office Unified Model by Walters et al. (2017) and found that the
106 radiation bias is reduced using the modified parameterization. Using ground-based
107 observations and retrievals, Xie and Zhang (2015) proposed a scale-aware cloud
108 inhomogeneity parameterization that they applied to the Community Earth System Model
109 (CESM) and found that it can recognize spatial scales without manual tuning. The
110 inhomogeneity parameter is essential in calculating enhancement factors and affect the
111 conversion rate from cloud to rain liquid. Xie and Zhang (2015), however, did not evaluate the
112 validity of CESM simulations from their parameterization; the effect of N_c variability or the
113 effect of covariance of cloud and rain on accretion process was not assessed. Most recently,
114 Zhang et al. (2018) derived the sub-grid CLWP and N_c from the MODIS cloud product. They
115 also studied the implication of the sub-grid cloud property variations for the autoconversion

116 rate simulation, in particular the enhancement factor, in GCMs. For the first time, the
117 enhancement factor due to ~~the~~ sub-grid variation of N_c is derived from satellite observation,
118 and results reveal several regions downwind of biomass burning aerosols (e.g., Gulf of Guinea,
119 East Coast of South Africa), air pollution (i.e., Eastern China Sea), and active volcanos (e.g.,
120 Kilauea, Hawaii and Ambae, Vanuatu), where the enhancement factor due to N_c is comparable,
121 or even larger than that due to CLWP. However, one limitation of Zhang et al. (2018) is the
122 use of passive remote sensing data only, which cannot distinguish cloud and rain water.

123 Dong et al. (2014a and 2014b) and Wu et al. (2015) reported MBL cloud and rain properties
124 over the Azores and provided the possibility of calculating the enhancement factors using
125 ground-based observations and retrievals. A joint retrieval method to estimate q_c and q_r profiles
126 is proposed based on existing studies and is presented in Appendix A. Most of the calculations
127 and analyses in this study is based on Morrison and Gettleman (2008, MG08 hereafter) scheme.
128 The enhancement factors in several other schemes are also discussed and compared with the
129 observational results and the approach in this study can be repeated for other microphysics
130 schemes in GCMs. This manuscript is organized as follows: section 2 includes a summary of
131 the mathematical formulas from previous studies that can be used to calculate grid-mean
132 process enhancement factors. Ground-based observations and retrievals are introduced in
133 Section 3. Section 4 presents results and discussions, followed by summary and conclusions in
134 Section 5. The retrieval method used in this study is in Appendix A.

135 2. Mathematical Background

136 Autoconversion and accretion rates in GCMs are usually parameterized as power law
 137 equations (Tripoli and Cotton, 1980; Beheng, 1994; Khairoutdinov and Kogan, 2000; Liu and
 138 Daum, 2004):

$$139 \left(\frac{\partial q_r}{\partial t} \right)_{auto} = A \bar{q}_c^{a1} \bar{N}_c^{a2}, \quad (1)$$

$$140 \left(\frac{\partial q_r}{\partial t} \right)_{accr} = B (\bar{q}_c \bar{q}_r)^b, \quad (2)$$

141 where A , $a1$, $a2$, B , and b are coefficients in different schemes listed in Table 1. The \bar{q}_c , \bar{q}_r ,
 142 and \bar{N}_c are grid-mean cloud water mixing ratio, rain water mixing ratio, and droplet number
 143 concentration, respectively. Because it is widely used in model parameterizations, the detailed
 144 results from Khairoutdinov and Kogan (2000) parameterization that been used in MG08
 145 scheme will be shown in Section 4 while a summary will be given for other schemes.

146 Ideally, the covariance between physical quantities should be considered in the calculation
 147 of both processes. However, \bar{q}_c and \bar{N}_c in Eq. (1) are arguably not independently retrieved in
 148 our retrieval method which will be introduced in this section and Appendix A. Thus we only
 149 assess the individual roles of q_c and N_c sub-grid variations in determining autoconversion rate.
 150 q_c and q_r , on the other hand, are retrieved from two independent algorithms as shown in Dong
 151 et al. (2014a and 2014b), Wu et al. (2015) and Appendix A, we will assess the effect of cloud
 152 and rain property covariance on accretion rate calculations.

153 In the sub-grid scale, the PDFs of q_c and N_c are assumed to follow a gamma distribution
 154 based on observational studies of optical depth in MBL clouds (Barker et al., 1996; Pincus et
 155 al., 1999; Wood and Hartmann, 2006):

$$156 \quad P(x) = \frac{\alpha^\nu}{\Gamma(\nu)} x^{\nu-1} e^{-\alpha x}, \quad (3)$$

157 where x represents q_c or N_c with grid-mean quantity \bar{q}_c or \bar{N}_c , represented by μ , $\alpha = \nu/\mu$ is the
 158 scale parameter, σ^2 is the relative variance of x (= variance divided by μ^2), $\nu = 1/\sigma^2$ is the
 159 shape parameter. ν is an indicator of cloud field homogeneity, with large values representing
 160 homogeneous and small values indicating inhomogeneous cloud field.

161 By integrating autoconversion rate, Eq. (1), over the grid-mean rate, Eq. (3), with respect
 162 to sub-grid scale variation of q_c and N_c , the autoconversion rate can be expressed as:

$$163 \quad \left(\frac{\partial q_r}{\partial t}\right)_{auto} = A \mu_{q_c}^{a1} \mu_{N_c}^{a2} \frac{\Gamma(\nu+a)}{\Gamma(\nu)\nu^a}, \quad (4)$$

164 where $a = a1$ or $a2$. Comparing Eq. (4) to Eq. (1), the autoconversion enhancement factor
 165 (E_{auto}) can be given with respect to q_c and N_c :

$$166 \quad E_{auto} = \frac{\Gamma(\nu+a)}{\Gamma(\nu)\nu^a}. \quad (5)$$

167 In addition to fitting the distributions of q_c and N_c , we also tried two other methods to
 168 calculate E_{auto} . The first is to integrate Eq. (1) over the actual PDFs from observed or retrieved
 169 parameters and the second is to fit a lognormal distribution for sub-grid variability like what
 170 has been done in other studies (e.g., Lebsock et al., 2013; Larson and Griffin, 2013). It is found

171 that all three methods get similar results. In this study, we use a gamma distribution that is
 172 consistent with MG08. Also note that, in the calculation of E_{auto} from \overline{N}_c , the negative exponent
 173 (-1.79) may cause singularity problems in Eq. (5). When this situation occurs, we do direct
 174 calculations by integrating the PDF of \overline{N}_c rather than using Eq. (5).

175 To account for the covariance of microphysical quantities in a model grid, it is difficult to
 176 apply bivariate gamma distribution due to its complex nature. In this study, the bivariate
 177 lognormal distribution of q_c and q_r is used (Lebsock et al., 2013; Boutle et al., 2014) and can
 178 be written as:

$$179 \quad P(\overline{q}_c, \overline{q}_r) = \frac{1}{2\pi\overline{q}_c\overline{q}_r\sigma_{q_c}\sigma_{q_r}\sqrt{1-\rho^2}} \exp\left\{-\frac{1}{2}\frac{1}{1-\rho^2}\left[\left(\frac{\ln\overline{q}_c-\mu_{q_c}}{\sigma_{q_c}}\right)^2 - 2\rho\left(\frac{\ln\overline{q}_c-\mu_{q_c}}{\sigma_{q_c}}\right)\left(\frac{\ln\overline{q}_r-\mu_{q_r}}{\sigma_{q_r}}\right) + \right.\right. \\ 180 \quad \left.\left.\left(\frac{\ln\overline{q}_r-\mu_{q_r}}{\sigma_{q_r}}\right)^2\right]\right\}, \quad (6)$$

181 where σ is standard deviation and ρ is the correlation coefficient of q_c and q_r .

182 Similarly, by integrating the accretion rate in Eq. (2) from Eq. (6), we get the accretion
 183 enhancement factor (E_{accr}) of:

$$184 \quad E_{accr} = \left(1 + \frac{1}{v_{q_c}}\right)^{\frac{1.15^2-1.15}{2}} \left(1 + \frac{1}{v_{q_r}}\right)^{\frac{1.15^2-1.15}{2}} \exp(\rho 1.15^2 \sqrt{\ln\left(1 + \frac{1}{v_{q_c}}\right) \ln\left(1 + \frac{1}{v_{q_r}}\right)}). \quad (7)$$

185 3. Ground-based observations and retrievals

186 The datasets used in this study were collected at the Department of Energy (DOE)
187 Atmospheric Radiation Measurement (ARM) Mobile Facility (AMF), which was deployed on
188 the northern coast of Graciosa Island (39.09°N, 28.03°W) from June 2009 to December 2010
189 (for more details, please refer to Rémillard et al., 2012; Dong et al., 2014a and Wood et al.,
190 2015). The detailed operational status of the remote sensing instruments on AMF was
191 summarized in Figure 1 of Rémillard et al. (2012) and discussed in Wood et al. (2015). The
192 ARM Eastern North Atlantic (ENA) site was established on the same island in 2013 and
193 provides long-term continuous observations.

194 The cloud-top heights (Z_{top}) were determined from W-band ARM cloud radar (WACR)
195 reflectivity and only single-layered low-level clouds with $Z_{top} \leq 3$ km are selected. Cloud-base
196 heights (Z_{base}) were detected by a laser ceilometer (CEIL) and the cloud thickness was simply
197 the difference between cloud top and base heights. The cloud liquid water path (CLWP) was
198 retrieved from microwave radiometer (MWR) brightness temperatures measured at 23.8 and
199 31.4 GHz using a statistical retrieval method with an uncertainty of 20 g m^{-2} for $CLWP < 200$
200 g m^{-2} , and 10% for $CLWP > 200 \text{ g m}^{-2}$ (Liljegren et al., 2001; Dong et al., 2000). Precipitating
201 status is identified through a combination of WACR reflectivity and Z_{base} . As in Wu et al.
202 (2015), we labelled the status of a specific time as “precipitating” if the WACR reflectivity
203 below the cloud base exceeds -37 dBZ.

204 The ARM merged sounding data have a 1-min temporal and 20-m vertical resolution below
205 3 km (Trojan, 2012). In this study, the merged sounding profiles are averaged to 5-min
206 resolution. Pressure and temperature profiles are used to calculate air density (ρ_{air}) profiles
207 and to infer adiabatic cloud water content.

208 Cloud droplet number concentration (N_c) is retrieved using the methods presented in Dong
209 et al. (1998, 2014a and 2014b) and are assumed to be constant in a cloud layer. Vertical profiles
210 of cloud and rain water content (CLWC and RLWC) are retrieved by combining WACR
211 reflectivity, CEIL attenuated backscatter and by assuming adiabatic growth of cloud parcels.
212 The detailed description is presented in Appendix A with the results from a selected case. The
213 CLWC and RLWC values are transformed to q_c and q_r by dividing by air density (e.g., $q_c(z) =$
214 $CLWC(z)/\rho_{air}(z)$).

215 The estimated uncertainties for the retrieved q_c and q_r are 30% and 18%, respectively (see
216 Appendix A). We used the estimated uncertainties of q_r and q_c as inputs of Eqs. (4) and (7) to
217 assess the uncertainties of E_{auto} and E_{accr} . For instance, $(1 \pm 0.3)q_c$ are used in Eq. (4) and the
218 mean differences are then used as the uncertainty of E_{auto} . Same method is used to estimate the
219 uncertainty for E_{accr} .

220 The autoconversion and accretion parameterizations partitioned from the collision-
221 coalescence process dominate at different levels in a cloud layer. Autoconversion dominates
222 around cloud top where cloud droplets reach maximum by condensation and accretion is

223 dominant at middle and lower parts of the cloud where rain drops sediment and continue to
224 grow by collecting cloud droplets. Complying with the physical processes, we estimate
225 autoconversion and accretion rates at different levels of a cloud layer in this study. The
226 averaged q_c within the top five range gates (~215 m thick) are used to calculate E_{auto} . To
227 calculate E_{accr} , we use the averaged q_c and q_r within five range gates around the maximum
228 radar reflectivity. If the maximum radar reflectivity appears at the cloud base, then five range
229 gates above the cloud base are used.

230 ~~The~~ ARM merged sounding data are also used to calculate lower tropospheric stability
231 ($LTS = \theta_{700 \text{ hPa}} - \theta_{1000 \text{ hPa}}$), which is used to infer ~~the~~ boundary layer stability. In this study,
232 unstable and stable boundary layers are defined as LTS less than 13.5 K and greater than 18 K,
233 respectively, and environment with an LTS between 13.5 K and 18 K is defined as mid-stable
234 (Wang et al. 2012; Bai et al. 2018). Enhancement factors in different boundary layers are
235 summarized in Section 4.2 and may be used as references for model simulations. Further, two
236 regimes are classified: CLWP greater than 75 g m^{-2} as precipitating and CLWP less than 75 g
237 m^{-2} as nonprecipitating (Rémillard et al., 2012).

238 To evaluate the dependence of autoconversion and accretion rates on sub-grid variabilities
239 for different model spatial resolutions, an averaged wind speed within a cloud layer was
240 extracted from merged sounding and used in sampling observations over certain periods to
241 mimic different grid sizes in GCMs. For example, two hours of observations corresponds to a

242 72-km grid box if mean in-cloud wind speed is 10 m s^{-1} horizontal wind and if the wind speed
243 is 5 m s^{-1} , four hours of observations is needed to mimic the same grid. We used six grid sizes
244 (30-, 60-, 90-, 120-, 150-, and 180-km) and mainly show the results from 60-km and 180-km
245 grid sizes in Section 4.

246 **4. Results and discussions**

247 In this section, we first show the data and methods using a selected case, followed by
248 statistical analysis based on 19 months of data and multiple time-intervals.

249 **4.1 Case study**

250 The selected case occurred on July 27, 2010 (Figure 1a) at the Azores. This case was
251 characterized by a long time of non-precipitating or light drizzling cloud development (00:00-
252 14:00 UTC) before intense drizzling occurred (14:00-20:00 UTC). Wu et al. (2017) studied
253 this case in detail to demonstrate the effect of wind shear on drizzle initiation. Here, we choose
254 two periods corresponding to a 180-km grid and having similar mean q_c near cloud top: 0.28 g
255 kg^{-1} for period c and 0.26 g kg^{-1} for period d but with different distributions (Figures 1c and
256 1d). The PDFs of q_c are then fitted using gamma distributions to get shape parameters (ν) as
257 shown in Figures 1c and 1d. Smaller ν is usually associated with a more inhomogeneous cloud
258 field, which allows more rapid drizzle production and more efficient liquid transformation from
259 cloud to rain (Xie and Zhang, 2015) in regions that satisfy precipitation criteria, which is
260 usually controlled using threshold q_r , droplet size or relative humidity (Kessler, 1969; Liu and

261 Daum, 2004). The period d has a wider q_c distribution than the period c, resulting in a smaller
262 ν and thus larger E_{auto} . Using the fitted ν , the E_{auto} from q_c is calculated from Eq. (5) and the
263 period d is larger than the period c (1.80 vs. 1.33). The E_{auto} values for the periods d and c can
264 also be calculated from N_c using the same procedure as q_c with a similar result (2.1 vs. 1.51).
265 The E_{accr} values for the periods d and c can be calculated from the covariance of q_c and q_r and
266 Eq. (7). Not surprisingly, the period d has larger E_{accr} than the period c. The combination of
267 larger E_{auto} and E_{accr} in the period d contributes to the rapid drizzle production and high rain
268 rate as seen from WACR reflectivity and q_r .

269 It is important to understand the physical meaning of enhancement factors in precipitation
270 parameterization. For example, if we assume two scenarios for q_c with a model grid having the
271 same mean values but different distributions: (1) The distribution is extremely homogeneous,
272 there will be no sub-grid variability because the cloud has the same chance to precipitate and
273 the enhancement factors would be unity (this is true for arbitrary grid-mean q_c amount as well).
274 (2) The cloud field gets more and more inhomogeneous with a broad range of q_c within the
275 model grid box, which results in a greater enhancement factor and increases the possibility of
276 precipitation. That is, a large enhancement factor can make the part of the cloud with higher q_c
277 within the grid box become more efficient in generating precipitation, rather than the entire
278 model grid.

279 Using the LWP retrieved from the Moderate Resolution Imaging Spectroradiometer
280 (MODIS) as an indicator of cloud ~~inhomogeneous~~, Wood and Hartmann (2006) found that
281 when clouds become more inhomogeneous, cloud fraction decreases, and open cells become
282 dominant with stronger ~~drizzling process~~ (Comstock et al., 2007). The relationship between
283 reduced homogeneity and stronger precipitation intensity is found in this study, which is similar
284 to ~~the~~ findings in other studies (e.g., Wood and Hartmann, 2006, Comstock et., 2007, Barker
285 et al., 1996; Pincus et al., 1999).

286 It is clear that q_c and N_c in Figure 1b are correlated with each other. In addition to their
287 natural relationships, q_c and N_c in our retrieval method are also correlated (Dong et al., 2014a
288 and 2014b). Thus, the effect of q_c and N_c covariance on E_{auto} is not included in this study. In
289 Figures 1c and 1d, the results are calculated using ~~model grid~~ of 180-km for the selected case
290 on 27 July 2010. In Section 4.2, we will use these approaches to calculate ~~their~~ statistical results
291 for multiple grid sizes using the 19-month ARM ground-based observations and retrievals.

292 **4.2 Statistical result**

293 For a specific grid size, e.g. 60-km, we estimate the shape parameter (ν) and calculate E_{auto}
294 through Eqns. (5) and (7). The PDFs of E_{auto} for both 60-km and 180-km grids are shown in
295 Figures 2a-2d. The distributions of E_{auto} values calculated from q_c with 60-km and 180-km grid
296 sizes (Figures 2a and 2b) are different ~~to each other~~ (2.79 vs. 3.3). The calculated E_{auto} values
297 range from 1 to 10, and most are less than 4. The average value for the 60-km grid (2.79) is

298 smaller than that for the 180-km grid (3.2), indicating a possible dependence of E_{auto} on model
299 grid size. Because drizzle-sized drops are primarily resulted from the autoconversion, we
300 investigate the relationship between E_{auto} and precipitation frequency, which is defined as the
301 average percentage of ~~drizzling~~ occurrence based on radar reflectivity below ~~the~~ cloud base.
302 Given the average LWP at Azores from Dong et al. (2014b, 109-140 g m⁻²), the precipitation
303 frequency (black lines in Figures 2a and 2b) agrees well with those from Kubar et al. (2009,
304 0.1-0.7 from their Figure 11). The precipitation frequency within each bin shows an increasing
305 trend for E_{auto} from 0 to 4-6, then oscillates around a **relative** constant when $E_{auto} > 6$, indicating
306 that in precipitation initiation process, E_{auto} keeps increasing to a certain value (~6) until the
307 precipitation frequency reaches a near-steady state. Larger E_{auto} values do not necessarily result
308 in higher precipitation frequency but instead may produce more drizzle-sized drops from
309 autoconversion process when the cloud is precipitating.

310 The PDFs of E_{auto} calculated from N_c also share similar patterns of positive skewness and
311 peaks at ~1.5-2.0 for the 60-km and 180-km grid sizes (Figures 2c and 2d). Although the
312 average values are close to their q_c counterparts (2.54 vs. 2.79 for 60-km and 3.45 vs. 3.2 for
313 180-km), the difference in E_{auto} between 60-km and 180-km grid sizes becomes large. The
314 precipitation frequencies within each bin are nearly constant or slightly decrease, which are
315 different to their q_c counterparts shown in Figures 2a and 2b. This suggests complicated effects
316 of droplet number concentration on precipitation initiation and warrants more explorations of

317 aerosol-cloud-precipitation interactions. This is very intriguing result, which suggests the
318 existence of significant sub-grid variation of N_c and this variation can significantly influence
319 the warm rain process. As mentioned in Section 2, q_c and N_c are also fitted using lognormal
320 distributions to calculate E_{auto} , those are close to the results in Figure 2 (not shown here) with
321 average values of 3.28 and 3.84, respectively, for 60-km and 180-km grid sizes. Because the
322 E_{auto} values calculated from q_c and N_c are close to each other, we will focus on analyzing the
323 results from q_c only for simplicity and clarity. The effect of q_c and N_c covariance, as stated in
324 Section 4.1, is not presented in this study due to the intrinsic correlation in the retrieval (Dong
325 et al., 2014a and 2014b and Appendix A of this study).

326 The covariance of q_c and q_r is included in calculating E_{accr} and the results are shown in
327 Figures 2e and 2f. The calculated E_{accr} values range from 1 to 4 with mean values of 1.62 and
328 1.76 for 60-km and 180-km grid sizes, respectively. These two mean values are much greater
329 than the prescribed value used in MG08 (1.07). Since accretion is dominant at middle and lower
330 parts of the cloud where rain drops sediment and continue to grow by collecting cloud droplets,
331 we superimpose the ratio of q_r to q_c within each bin (black lines in Figures 2e and 2f) to
332 represent the portion of rain water in the cloud layer. In both panels, the ratios are less than
333 15%, which means that q_r can be one order of magnitude smaller than q_c . The differences in
334 magnitude are consistent with previous CloudSat and aircraft results (e.g., Boutle et al., 2014).
335 This ratio increases from $E_{accr}=0$ to ~ 2 , and then decreases, suggesting a possible optimal state

336 for the collision-coalescence process to achieve maximum efficiency for converting cloud
337 water into rain water at $E_{accr}=2$. In other words, the conversion efficiency cannot be infinitely
338 increased with E_{accr} under available cloud water. The ratio of q_r to q_c increases from $E_{accr}=1.07$
339 (0.063) to $E_{accr}=2.0$ (0.142), indicating that the fraction of rain water in total water using the
340 prescribed E_{accr} is too low. This ratio could be increased significantly using a large E_{accr} value,
341 therefore increasing precipitation intensity in the models. This further ~~proves~~ that the
342 prescribed value of $E_{accr}=1.07$ used in MG08 is too small to correctly simulate precipitation
343 intensity in the models. Therefore, similar to the conclusions in Lebosck et al. (2013) and
344 Boutle et al. (2014), we suggest increasing E_{accr} from 1.07 to 1.5-2.0 in GCMs.

345 To illustrate the impact of using prescribed enhancement factors, autoconversion and
346 accretion rates are calculated using the prescribed values (e.g., 3.2 for E_{auto} and 1.07 for E_{accr} ,
347 MG08; Xie and Zhang, 2015) and the newly calculated ones ~~in~~ Figure 2 ~~that use~~ observations
348 and retrievals. Figure 3 shows the joint density of autoconversion (Figures 3a and 3b) and
349 accretion rates (Figures 3c and 3d) from observations (x-axis) and model parameterizations (y-
350 axis) for 60-km and 180-km grid sizes. Despite the spread, the peaks of the joint density of
351 autoconversion rate appear slightly above the one-to-one line, suggesting that cloud droplets in
352 the model are more easily ~~to be~~ converted into drizzle/rain drops than observations. On the
353 other hand, the peaks of accretion rate appear slightly below the one-to-one line which indicates
354 that simulated precipitation intensities are lower than observed ones. The magnitudes of the

355 two rates are consistent with Khairoutdinov and Kogan (2000), Liu and Daum (2004), and
356 Wood (2005b).

357 Compared to the observations, ~~the~~ precipitation in GCMs occurs at higher frequencies with
358 lower intensities, which might explain why the total precipitation amounts are close to surface
359 measurements over an entire grid box. This ‘promising’ result, however, fails to simulate
360 precipitation on the right scale and cannot capture the correct rain water amount, thus providing
361 limited information in estimating rain water evaporation and air-sea energy exchange.

362 Clouds in an unstable boundary layer have a better chance of getting moisture supply from
363 the surface by upward motion than clouds in a stable boundary layer. Precipitation frequencies
364 are thus different in these two boundary layer regimes. For example, clouds in a relatively
365 unstable boundary layer more easily produce drizzle than those in a stable boundary layer (Wu
366 et al., 2017). Provided the same boundary layer condition, CLWP is an important factor in
367 determining the precipitation ~~status~~ of clouds. At the Azores, precipitating clouds are more
368 likely to have CLWP greater than 75 g m^{-2} than their nonprecipitating counterparts (Rémillard
369 et al., 2012). To further investigate what conditions and parameters **can** significantly influence
370 the enhancement factors, we classify low-level clouds according to their boundary layer
371 conditions and CLWPs.

372 The averaged E_{auto} and E_{accr} values for each category are listed in Table 2. Both E_{auto} and
373 E_{accr} increase when the boundary layer becomes less stable, and these values become larger in

374 precipitating clouds ($CLWP > 75 \text{ gm}^{-2}$) than those in nonprecipitating clouds ($CLWP < 75 \text{ gm}^{-2}$).
375 In real applications, autoconversion process only occurs when q_c or cloud droplet size reaches
376 a certain threshold (e.g., Kessler, 1969 and Liu and Daum, 2004). Thus, it will not affect model
377 simulations if a valid E_{auto} is assigned to Eq. (1) in a nonprecipitating cloud. The E_{auto} values
378 in both stable and mid-stable boundary layer conditions are smaller than the prescribed value
379 of 3.2, while the values in unstable boundary layers are significantly larger than 3.2 regardless
380 of if they are precipitating or not. All E_{accr} values are greater than the constant of 1.07. The
381 E_{auto} values in Table 2 range from 2.32 to 6.94 and the E_{accr} values vary from 1.42 to 1.86,
382 depending on different boundary layer conditions and CLWPs. Therefore, as suggested by Hill
383 et al. (2015), the selection of E_{auto} and E_{accr} values in GCMs should be regime-dependent.

384 To properly parameterize sub-grid variabilities, the approaches by Hill et al. (2015) and
385 Walters et al. (2017) can be adopted. To use MG08 and other parameterizations in GCMs as
386 listed in Table 1, proper adjustments can be made according to the model grid size, boundary
387 layer conditions, and precipitating status. As stated in the methodology, we used a variety of
388 model grid sizes. Figure 4 demonstrates the dependence of both enhancement factors on
389 different model grid sizes. The E_{auto} values (red line) increase from 1.97 at a grid box of 30×30
390 km to 3.15 at a grid box of 120×120 km, which are 38.4% and 2% percent lower than the
391 prescribed value (3.2, upper dashed line). After that, the E_{auto} values remain relatively constant
392 at ~ 3.18 when the model grid is 180 km, which is close to the prescribed value of 3.2 used in

393 MG08. This result indicates that the prescribed value in MG08 represents well in large grid
394 sizes in GCMs. The E_{accr} values (blue line) increase from 1.53 at a grid box of 30×30 km to
395 1.76 at a grid box of 180×180 km, those are 43% and 64%, respectively, larger than the
396 prescribed value (1.07, lower dashed line). The shaded areas represent the uncertainties of E_{auto}
397 and E_{accr} associated with the uncertainties of the retrieved q_c and q_r . When model grid size
398 increases, the uncertainties slightly decrease. The prescribed E_{auto} is close to the upper
399 boundary of uncertainties except for the 30-km grid size, while the prescribed E_{accr} is
400 significantly lower than the lower boundary.

401 It is noted that E_{auto} and E_{accr} depart from their prescribed values at opposite directions as
402 model grid size increases. For models with finer resolutions (e.g., 30-km), both E_{auto} and E_{accr}
403 are significantly different from the prescribed values, which can partially explain the issue of
404 ‘too frequent’ and ‘too light’ precipitation. Under both conditions, the accuracy of precipitation
405 estimation is degraded. For models with coarser resolutions (e.g., 180-km), average E_{auto} is
406 exactly 3.2 while E_{accr} is much larger than 1.07 when compared to finer resolution simulations.
407 In such situations, the simulated precipitation will be dominated by the ‘too light’ problem, in
408 addition to regime-dependent (Table 2) and as in Xie and Zhang (2015), E_{auto} and E_{accr} should
409 be also scale-dependent.

410 Also note that the location we choose to collect ground-based observations and retrievals is
411 on the remote ocean where the MBL clouds mainly form in a relatively stable boundary layer

412 and are characterized by high precipitation frequency. Even in such environments, however,
413 ~~the~~ GCMs overestimate the precipitation frequency (Ahlgrimm and Forbes, 2014).

414 To further investigate how enhancement factors affect precipitation simulations, we use
415 E_{auto} as a fixed value of 3.2 in Eq. (4), and then calculate the q_c needed for models to reach the
416 same autoconversion rate as observations. The q_c differences between models and observations
417 are then calculated, which represent the q_c adjustment in models to get a realistic
418 autoconversion rate in the simulations. Similar to Figure 1, the PDFs of q_c differences (model
419 – observation) are plotted in Figures 5a and 5b for 60-km and 180-km grid sizes. Figure 5c
420 shows the average percentages of model q_c adjustments for different model grid sizes. The
421 mode and average values for 30-km grid is negative, suggesting that models need to simulate
422 lower q_c in general to get reasonable autoconversion rates. Lower q_c values are usually
423 associated with smaller E_{auto} values that induce lower simulated precipitation frequency. On
424 average, the ~~percentage~~ of q_c adjustments decrease with increasing model grid size. For
425 example, the adjustments for finer resolutions (e.g., 30-60 km) can be ~20% ~~of the~~ q_c , whereas
426 adjustments in coarse resolution models (e.g., 120 – 180 km) are relatively small because the
427 prescribed E_{auto} (=3.2) is close to the observed ones (Figure 4) and when model grid size is
428 180-km, no adjustment is needed. The adjustment method presented in Figure 5, however, may
429 change cloud water substantially and may cause a variety of subsequent issues, such as altering
430 cloud radiative effects and disrupting the hydrological cycle. The assessment in Figure 5 only

431 provides a reference to the equivalent effect on cloud water by using the prescribed E_{auto} value
432 as compared to those from observations.

433 All above discussions are based on the prescribed E_{auto} and E_{accr} values (3.2 and 1.07) in
434 **MG08. Whereas** there are quite a few parameterizations that have been published so far. In this
435 study, we list E_{auto} and E_{accr} for three other widely used parameterization schemes in Table 3,
436 which are given only for 60-km and 180-km grid sizes. The values of the exponent in each
437 scheme directly affect the values of the enhancement factors. For example, the scheme in
438 Beheng (1994) has highest degree of nonlinearity and hence has the largest enhancement
439 factors. The scheme in Liu and Daum (2004) is very similar to the scheme in Khairoutdinov
440 and Kogan (2000) because both schemes have a physically realistic dependence on cloud water
441 content and number concentration (Wood, 2005b). For a detailed overview and discussion of
442 various existing parameterizations, please refer to Liu and Daum (2004), Liu et al. (2006a), Liu
443 et al. (2004b), Wood (2005b) and Michibata and Takemura (2015). A physical based
444 autoconversion parameterization was developed by Lee and Baik (2017) in which the scheme
445 was derived by solving stochastic collection equation with an approximated collection kernel
446 that is constructed using the terminal velocity of cloud droplets and the collision efficiency
447 obtained from a particle trajectory model. Due to the greatly increased complexity of their
448 equation, we do not attempt to calculate E_{auto} here **but should** be examined in future studies due
449 to the physics feasibility of the Lee and Baik (2017) scheme.

450

451 **5. Summary**

452 To better understand the influence of sub-grid cloud variations on the warm-rain process
453 simulations in GCMs, we investigated the warm-rain parameterizations of autoconversion
454 (E_{auto}) and accretion (E_{accr}) enhancement factors in MG08. These two factors represent the
455 effects of sub-grid cloud and precipitation variabilities when parameterizing autoconversion
456 and accretion rates as functions of grid-mean quantities. E_{auto} and E_{accr} are prescribed as 3.2
457 and 1.07, respectively, in the widely used MG08 scheme. To assess the dependence of the two
458 parameters on sub-grid scale variabilities, we used ground-based observations and retrievals
459 collected at the DOE ARM Azores site to reconstruct the two enhancement factors in different
460 model grid sizes.

461 From the retrieved q_c and q_r profiles, the averaged q_c within the top five range gates are
462 used to calculate E_{auto} and the averaged q_c and q_r within five range gates around maximum
463 reflectivity are used to calculate E_{accr} . The calculated E_{auto} values from observations and
464 retrievals increase from 1.96 at a grid box of 30×30 km to 3.15 at a grid box of 120×120 km.
465 These values are 38% and 2% lower than the prescribed value of 3.2. The prescribed value in
466 MG08 represents well in large grid sizes in GCMs. On the other hand, the E_{accr} values increase
467 from 1.53 at a grid box of 30×30 km to 1.76 at a grid box of 180×180 km, which are 43% and
468 64% higher than the prescribed value (1.07). The higher E_{auto} and lower E_{accr} prescribed in

469 GCMs help to explain the issue of too frequent precipitation events with too light precipitation
470 intensity. The ratios of rain to cloud liquid water increase with increasing E_{accr} from 0 to 2, and
471 then decrease after that, suggesting a possible optimal state for the collision-coalescence
472 process to achieve maximum efficiency for converting cloud water into rain water at $E_{accr}=2$.
473 The ratios of q_r to q_c at $E_{accr}=1.07$ and $E_{accr}=2.0$ are 0.063 and 0.142, further proving that the
474 prescribed value of $E_{accr}=1.07$ is too small to simulate correct precipitation intensity in models.

475 To further investigate what conditions and parameters can significantly influence the
476 enhancement factors, we classified low-level clouds according to their boundary layer
477 conditions and CLWPs. Both E_{auto} and E_{accr} increase when the boundary layer conditions
478 become less stable, and the values are larger in precipitating clouds ($CLWP>75 \text{ gm}^{-2}$) than
479 those in nonprecipitating clouds ($CLWP<75 \text{ gm}^{-2}$). The E_{auto} values in both stable and mid-stable
480 boundary layer conditions are smaller than the prescribed value of 3.2, while those in unstable
481 boundary layers conditions are significantly larger than 3.2 regardless of whether or not the
482 cloud is precipitating (Table 2). All E_{accr} values are greater than the prescribed value of 1.07.
483 Therefore, the selection of E_{auto} and E_{accr} values in GCMs should be regime-dependent, which
484 also has been suggested by Hill et al. (2015) and Walters et al. (2017).

485 This study, however, did not include the effect of uncertainties in GCM simulated cloud
486 and precipitation properties on sub-grid scale variations. For example, we did not consider the
487 behavior of the two enhancement factors under different aerosol regimes, a condition which

488 may affect precipitation formation process. The effect of aerosol-cloud-precipitation-
489 interactions on cloud and precipitation sub-grid variabilities may be of comparable importance
490 to meteorological regimes and precipitation status and deserves a further study. Other than the
491 large-scale dynamics, e.g., LTS in this study, ~~upward/downward motion in sub-grid scale~~
492 also modify cloud and precipitation development and affect the calculations of enhancement
493 factors. ~~The~~ investigation of the dependence of E_{auto} and E_{accr} on aerosol type and concentration
494 as well as on vertical velocity would be a natural extension and complement of current study.
495 In addition, other factors may also affect precipitation frequency and intensity even under the
496 same aerosol regimes and even if the clouds have similar cloud water contents. Wind shear, for
497 example as presented in Wu et al. (2017), is an external variable that can affect precipitation
498 formation. Further studies are needed to evaluate the role of the covariance of q_c and N_c in sub-
499 grid scales on E_{auto} determinations, which is beyond the scope of this study and requires
500 independent retrieval techniques.

501

502 **Appendix A: Joint cloud and rain LWC profile estimation**

503 If a time step is identified as non-precipitating, the cloud liquid water content (CLWC)
504 profile is retrieved using Frisch et al. (1995) and Dong et al. (1998, 2014a and 2014b). The
505 retrieved CLWC is proportional to radar reflectivity.

506 If a time step is identified as precipitating (maximum reflectivity below cloud base
 507 exceeds -37 dBZ), CLWC profile is first inferred from temperature and pressure in merged
 508 sounding by assuming adiabatic growth. Marine stratocumulus is close to adiabatic (Albrecht
 509 et al. 1990) and was used in cloud property retrievals in literature (e.g., Rémillard et al., 2013).
 510 In this study, we use the information from rain properties near cloud base to further constrain
 511 the adiabatic CLWC ($CLWC_{adiabatic}$).

512 Adopting the method of O'Connor et al. (2005), Wu et al. (2015) retrieved rain properties
 513 below cloud base (CB) for the same period as in this study. In Wu et al. (2015), rain drop size
 514 (median diameter, D_0), shape parameter (μ), and normalized rain droplet number concentration
 515 (N_W) are retrieved for the assumed rain particle size distribution (PSD):

$$516 \quad n_r(D) = N_W f(\mu) \left(\frac{D}{D_0}\right)^\mu \exp\left[-\frac{(3.67+\mu)D}{D_0}\right] \quad (A1)$$

517 To infer rain properties above cloud base, we adopt the assumption in Fielding et al. (2015)
 518 that N_W increases from below CB to within the cloud. This assumption is consistent with the *in*
 519 *situ* measurement in Wood (2005a). Similar as Fielding et al. (2015), we use constant N_W within
 520 cloud if the N_W decrease with height below CB. The μ within cloud is treated as constant and
 521 is taken as the averaged value from four range gates below CB. Another assumption in the
 522 retrieval is that the evaporation of rain drops is negligible from one range gate above CB to one
 523 range gate below CB thus we assume rain drop size is the same at the range gate below and
 524 above CB.


525 With the above information, we can calculate the reflectivity contributed by rain at the first
 526 range gate above CB ($Z_d(1)$) and the cloud reflectivity ($Z_c(1)$) is then $Z_c(1) = Z(1) - Z_d(1)$,
 527 where $Z(1)$ is WACR measured reflectivity at first range gate above CB. Using cloud droplet
 528 number concentration (N_c) from Dong et al. (2014a and 2014b), CLWC at the first range gate
 529 above CB can be calculated through

$$530 \quad Z_c(1) = 2^6 \int_0^\infty n_c(r) r^6 dr = \frac{36}{\pi^2 \rho_w^2} \frac{CLWC(1)_{reflectivity}^2}{N_c} \exp(9\sigma_x^2) \quad (A2)$$

531 where $n_c(r)$ is lognormal distribution of cloud PSD with logarithmic width σ_x which is set to
 532 a constant value of 0.38 (Miles et al., 2000), ρ_w is liquid water density.

533 We then compare the $CLWC_{adiabatic}$ and the one calculated from $CLWC_{reflectivity}$ at the
 534 first range gate above CB. A scale parameter (s) is defined as $s = \frac{CLWC_{reflectivity}(1)}{CLWC_{adiabatic}(1)}$ and the
 535 entire profile of $CLWC_{adiabatic}$ is multiplied by s to correct the bias from cloud sub-
 536 adiabaticity. Reflectivity profile from cloud is then calculated from Eq. (A2) and the remaining
 537 reflectivity profile from WACR observation is regarded as rain contribution. Rain particle size
 538 can then be calculated given that N_w and μ are known and rain liquid water content (RLWC)
 539 can be estimated.

540 There are two constraints used in the retrieval. One is that the summation of cloud and rain
 541 liquid water path (CLWP and RLWP) must be equal to the LWP from microwave radiometer
 542 observation. Another is that rain drop size (D_0) near cloud top must be equal or greater than 50

543 μm and if D_0 is less than $50 \mu m$, we decrease N_W for the entire rain profile within cloud and
544 repeat the calculation until the $50 \mu m$ criteria is satisfied. 

545 It is difficult to quantitatively estimate the retrieval uncertainties without aircraft in situ
546 measurements. For the proposed retrieval method, 18% should be used as uncertainty for
547 RLWC from rain properties in Wu et al. (2015) and 30% for CLWC from cloud properties in
548 Dong et al. (2014a and 2014b). The actual uncertainty depends on the accuracy of merged
549 sounding data, the detectability of WACR near cloud base and the effect of entrainment on
550 cloud adiabaticity during ~~precipitating~~. In the recent aircraft field campaign, the Aerosol and
551 Cloud Experiments in Eastern North Atlantic (ACE-ENA) was conducted during 2017-2018
552 with a total of 39 flights over the Azores, near the ARM ENA site on Graciosa Island. These
553 aircraft in situ measurements will be used to validate the ground-based retrievals and
554 quantitatively estimate their uncertainties in the future.

555 Figure A1 shows an example of the retrieval results. The merged sounding, ceilometer,
556 microwave radiometer, WACR and ceilometer are used in the retrieval. Whenever one or more
557 instruments are not reliable, that time step is skipped, and this results in the gaps in the CLWC
558 and RLWC as shown in Figures A1(b) and A1(c). When the cloud is classified as
559 nonprecipitating, no RLWC ~~will be~~ retrieved ~~as well~~. Using air density (ρ_{air}) profiles
560 calculated from temperature and pressure in merged sounding, mixing ratio (q) can be
561 calculated from LWC using $q(z) = LWC(z)/\rho_{air}(z)$.

562 **Acknowledgements**

563 The ground-based measurements were obtained from the Atmospheric Radiation Measurement
564 (ARM) Program sponsored by the U.S. Department of Energy (DOE) Office of Energy
565 Research, Office of Health and Environmental Research, and Environmental Sciences
566 Division. The data can be downloaded from <http://www.archive.arm.gov/>. This research was
567 supported by the DOE CESM project under grant DE-SC0014641 at the University of Arizona
568 through subaward from University of Maryland at Baltimore County, and the NSF project
569 under grant AGS-1700728 at University of Arizona. The authors thank Dr. Yangang Liu at
570 Brookhaven National Laboratory for insightful comments and Ms. Casey E. Oswant at the
571 University of Arizona for proof reading the manuscript. The two anonymous reviewers are
572 acknowledged for constructive comments and suggestions which helped to improve the
573 manuscript.

574

575 **References**

576 Ackerman, A. S., Kirkpatrick, M. P., Stevens, D. E., and Toon, O. B.: The impact of humidity
577 above stratiform clouds on indirect aerosol climate forcing, *Nature*, 432, 1014–1017, 2004.
578 Ahlgrim, M., and Forbes, R.: Improving the Representation of Low Clouds and Drizzle in
579 the ECMWF Model Based on ARM Observations from the Azores, *J. Clim.*, doi:
580 10.1175/MWR-D-13-00153.1, 2014.
581 Albrecht, B. A.: Aerosols, cloud microphysics, and fractional cloudiness, *Science*, 245, 1227–
582 1231, 1989.

- 583 Albrecht, B., Fairall, C., Thomson, D., White, A., Snider, J., and Schubert, W.: Surface-based
584 remote-sensing of the observed and the adiabatic liquid water-content of stratocumulus
585 clouds, *Geophys. Res. Lett.*, 17, 89–92, doi:10.1029/G1017i001p00089, 1990.
- 586 Austin, P., Wang, Y., Kujala, V., and Pincus, R.: Precipitation in Stratocumulus Clouds:
587 Observational and Modeling Results, *J. Atmos. Sci.*, 52, 2329–2352, doi:10.1175/1520-
588 0469(1995)052<2329:PISCOA>2.0.CO;2, 1995.
- 589 Bai, H., Gong, C., Wang, M., Zhang, Z., and L'Ecuyer, T.: Estimating precipitation
590 susceptibility in warm marine clouds using multi-sensor aerosol and cloud products from
591 A-Train satellites, *Atmos. Chem. Phys.*, 18, 1763-1783, [https://doi.org/10.5194/acp-18-](https://doi.org/10.5194/acp-18-1763-2018)
592 1763-2018, 2018.
- 593 Barker H. W., Wiellicki B.A., Parker L.: A parameterization for computing grid-averaged solar
594 fluxes for inhomogeneous marine boundary layer clouds. Part II: Validation using satellite
595 data. *J. Atmos. Sci.* 53: 2304–2316, 1996.
- 596 Beheng, K. D.: A parameterization of warm cloud microphysical conversion processes, *Atmos.*
597 *Res.*, 33, 193-206, 1994.
- 598 Bony, S., and Dufresne, J.-L.: Marine boundary layer clouds at the heart of tropical cloud
599 feedback uncertainties in climate models, *Geophys. Res. Lett.*, 32, L20806,
600 doi:10.1029/2005GL023851, 2005.
- 601 Boutle, I. A., Abel, S. J., Hill, P. G., and Morcrette, C. J.: Spatial variability of liquid cloud and
602 rain: Observations and microphysical effects. *Quart. J. Roy. Meteor. Soc.*, 140, 583–594,
603 doi:10.1002/qj.2140, 2014.
- 604 Chen, T., Rossow, W. B., and Zhang, Y.: Radiative Effects of Cloud-Type Variations, *J. Clim.*,
605 13, 264–286, 2000.
- 606 Cheng, A., and Xu. K.-M.: A PDF-based microphysics parameterization for simulation of
607 drizzling boundary layer clouds, *J. Atmos. Sci.*, 66, 2317–2334,
608 doi:10.1175/2009JAS2944.1, 2009.

- 609 Comstock, K. K., Yuter, S. E., Wood, R., and Bretherton, C. S.: The Three-Dimensional
610 Structure and Kinematics of Drizzling Stratocumulus, *Mon. Weather Rev.*, 135, 3767–
611 3784, doi:10.1175/2007MWR1944.1, 2007.
- 612 Dong X., Ackerman, T. P., and Clothiaux, E. E.: Parameterizations of Microphysical and
613 Radiative Properties of Boundary Layer Stratus from Ground-based measurements, *J.*
614 *Geophys. Res.*, 102, 31,681-31,393, 1998.
- 615 Dong, X., Minnis, P., Ackerman, T. P., Clothiaux, E. E., Mace, G. G., Long, C. N., and
616 Liljegren, J. C.: A 25-month database of stratus cloud properties generated from ground-
617 based measurements at the ARM SGP site, *J. Geophys. Res.*, 105, 4529-4538, 2000.
- 618 Dong, X., Xi, B., Kennedy, A., Minnis, P. and Wood, R.: A 19-month Marine Aerosol-
619 Cloud_Radiation Properties derived from DOE ARM AMF deployment at the Azores:
620 Part I: Cloud Fraction and Single-layered MBL cloud Properties, *J. Clim.*, 27,
621 doi:10.1175/JCLI-D-13-00553.1, 2014a.
- 622 Dong, X., Xi, B., and Wu, P.: Investigation of Diurnal Variation of MBL Cloud Microphysical
623 Properties at the Azores, *J. Clim.*, 27, 8827-8835, 2014b.
- 624 Fielding, M. D., Chiu, J. C., Hogan, R. J., Feingold, G., Eloranta, E., O'Connor, E. J. and
625 Cadetdu, M. P.: Joint retrievals of cloud and drizzle in marine boundary layer clouds using
626 ground-based radar, lidar and zenith radiances. *Atmospheric Measurement Techniques*, 8,
627 pp. 2663-2683. ISSN 1867-8548 doi: 10.5194/amt-8-2663-2015, 2015.
- 628 Frisch, A., Fairall, C., and Snider, J.: Measurement of stratus cloud and drizzle parameters in
629 ASTEX with a Ka-band Doppler radar and a microwave radiometer, *J. Atmos. Sci.*, 52,
630 2788–2799, 1995.
- 631 Hahn, C. and Warren, S.: A gridded climatology of clouds over land (1971–96) and ocean
632 (1954–97) from surface observations worldwide, Numeric Data Package NDP-026E
633 ORNL/CDIAC-153, CDIAC, Department of Energy, Oak Ridge, Tennessee, 2007.

- 634 Hartmann, D. L., Ockert-Bell, M. E., and Michelsen, M. L.: The Effect of Cloud Type on
635 Earth's Energy Balance: Global Analysis, *J. Climate*, 5, 1281–1304,
636 [https://doi.org/10.1175/15200442\(1992\)005<1281:TEOCTO>2.0.CO;2](https://doi.org/10.1175/15200442(1992)005<1281:TEOCTO>2.0.CO;2), 1992.
- 637 Hartmann, D. L. and Short, D. A.: On the use of earth radiation budget statistics for studies of
638 clouds and climate, *J. Atmos. Sci.*, 37, 1233–1250, doi:10.1175/1520-
639 0469(1980)037<1233:OTUOER>2.0.CO;2, 1980.
- 640 Hill, P. G., Morcrette, C. J., and Boutle, I. A.: A regime-dependent parametrization of subgrid-
641 scale cloud water content variability, *Q. J. R. Meteorol. Soc.*, 141, 1975–1986, 2015.
- 642 Houghton, J. T., Ding, Y., Griggs, D.J., Noguer, M., van der Linden, P.J., Dai, X., Maskell, K.,
643 and Johnson, C.A.: *Climate Change: The Scientific Basis*, Cambridge University Press,
644 881 pp, 2001.
- 645 Jess, S.: Impact of subgrid variability on large-scale precipitation formation in the climate
646 model ECHAM5, PhD thesis, Dep. of Environ. Syst. Sci., ETH Zurich, Zurich,
647 Switzerland, 2010.
- 648 Jiang, J., Su, H., Zhai, C., Perun, V. S., Del Genio, A., Nazarenko, L. S., Donner, L. J.,
649 Horowitz, Seman, L., Cole, C., J., Gettelman, A., Ringer, M. A., Rotstayn, L., Jeffrey, S.,
650 Wu, T., Brient, F., Dufresne, J-L., Kawai, H., Koshiro, T., Watanabe, M., LÉcuyer, T. S.,
651 Volodin, E. M., Iversen, Drange, T., H., Mesquita, M. D. S., Read, W. G., Waters, J. W.,
652 Tian, B., Teixeira, J., and Stephens, G. L.: Evaluation of cloud and water vapor simulations
653 in CMIP5 climate models using NASA “A-train” satellite observations, *J. Geophys. Res.*,
654 117, D14105, doi:10.1029/2011JD017237, 2012.
- 655 Kessler, E.: On the distribution and continuity of water substance in atmospheric circulations,
656 *Met. Monograph* 10, No. 32, American Meteorological Society, Boston, USA, 84 pp.,
657 1969.
- 658 Khairoutdinov, M. and Kogan, Y.: A New Cloud Physics Parameterization in a Large-Eddy
659 Simulation Model of Marine Stratocumulus, *Mon. Wea. Rev.*, 128, 229-243, 2000.

- 660 Kooperman, G. J., Pritchard, M. S., Ghan, S. J., Wang, M., Somerville, R. C., and Russell, L.
661 M.: Constraining the influence of natural variability to improve estimates of global aerosol
662 indirect effects in a nudged version of the Community Atmosphere Model 5, *J. Geophys.*
663 *Res.*, 117, D23204, <https://doi.org/10.1029/2012JD018588>, 2012.
- 664 Kubar, T. L., Hartmann, D. L., and Wood, R.: Understanding the importance of microphysics
665 and macrophysics in marine low clouds, Part I: satellite observations. *J. Atmos. Sci.*, 66,
666 2953-2972, doi: 10.1175/2009JAS3071.1, 2009.
- 667 Larson, V. E., Nielsen, B. J., Fan, J., and Ovchinnikov, M.: Parameterizing correlations
668 between hydrometeor species in mixed-phase Arctic clouds, *J. Geophys. Res.*, 116,
669 D00T02, doi:10.1029/2010JD015570, 2011.
- 670 Larson, V. E., and Griffin, B. M.: Analytic upscaling of a local microphysics scheme. Part I:
671 Derivation. *Quart. J. Roy. Meteor. Soc.*, 139, 46–57, 2013.
- 672 Lebsock, M. D., Morrison, H., and Gettelman, A.: Microphysical implications of cloud-
673 precipitation covariance derived from satellite remote sensing, *J. Geophys. Res.-Atmos.*,
674 118, 6521–6533, <https://doi.org/10.1002/jgrd.50347>, 2013.
- 675 Lee, H., and Baik, J.-J.: A physically based autoconversion parameterization. *Journal of the*
676 *Atmospheric Sciences*, 74, 1599–1616, 2017.
- 677 Leon, D. C., Wang, Z., and Liu, D.: Climatology of drizzle in marine boundary layer clouds
678 based on 1 year of data from CloudSat and Cloud-Aerosol Lidar and Infrared Pathfinder
679 Satellite Observations (CALIPSO), *J. Geophys. Res.*, 113, D00A14,
680 doi:10.1029/2008JD009835, 2008.
- 681 Liljegren, J. C., Clothiaux, E. E., Mace, G. G., Kato, S., and Dong, X.: A new retrieval for
682 cloud liquid water path using a ground-based microwave radiometer and measurements of
683 cloud temperature, *J. Geophys. Res.*, 106, 14,485-14,500, 2001.
- 684 Liu, Y. and Daum, P. H.: Parameterization of the autoconversion process, Part I: Analytical
685 formulation of the Kessler-type parameterizations, *J. Atmos. Sci.*, 61, 1539–1548, 2004.

- 686 Liu, Y., Daum, P. H., and McGraw, R.: Parameterization of the autoconversion process. Part
687 II: Generalization of Sundqvist-type parameterizations, *J. Atmos. Sci.*, 63, 1103–1109,
688 2006a.
- 689 Liu, Y., Daum, P. H., McGraw, R., Miller, M.: Generalized threshold function accounting for
690 effect of relative dispersion on threshold behavior of autoconversion process. *Geophys.*
691 *Res. Lett.*, 33, L11804, 2006b.
- 692 Lohmann, U. and Feichter, J.: Global indirect aerosol effects: a review, *Atmos. Chem. Phys.*,
693 5, 715–737, doi:10.5194/acp-5-715-2005, 2005.
- 694 Michibata, T., and Takemura, T.: Evaluation of autoconversion schemes in a single model
695 framework with satellite observations, *J. Geophys. Res. Atmos.*, 120, 9570–9590,
696 doi:10.1002/2015JD023818, 2015.
- 697 Miles, N. L., Verlinde, J., and Clothiaux, E. E.: Cloud-droplet size distributions in low-level
698 stratiform clouds. *J. Atmos. Sci.*, 57, 295–311, doi:10.1175/1520-0469(2000)057,
699 0295:CDS DIL.2.0.CO;2, 2000.
- 700 Morrison, H. and Gettelman, A.: A new two-moment bulk stratiform cloud microphysics
701 scheme in the Community Atmosphere Model, version 3 (CAM3). Part I: Description and
702 numerical tests, *J. Climate*, 21, 3642–3659, 2008.
- 703 Nam, C., and Quaas, J.: Evaluation of clouds and precipitation in the ECHAM5 general
704 circulation model using CALIPSO and CloudSat satellite data, *J. Clim.*, 25, 4975–4992,
705 doi:10.1175/JCLI-D-11-00347.1, 2012.
- 706 O’Connor, E. J., Hogan, R. J., and Illingworth, A. J.: Retrieving stratocumulus drizzle
707 parameters using Doppler radar and lidar, *J. of Applied Meteorol.*, 44, 14-27, 2005.
- 708 Pincus, R., McFarlane, S. A., and Klein, S. A.: Albedo bias and the horizontal variability of
709 clouds in subtropical marine boundary layers: Observations from ships and satellites, *J.*
710 *Geophys. Res.*, 104, 6183–6191, doi:10.1029/1998JD200125, 1999.

- 711 Pincus, R., and Klein, S. A.: Unresolved spatial variability and microphysical process rates in
712 large-scale models. *J. Geophys. Res.*, 105D, 27 059–27 065, 2000.
- 713 Quaas, J., Ming, Y., Menon, S., Takemura, T., Wang, M., Penner, J. E., Gettelman, A.,
714 Lohmann, U., Bellouin, N., Boucher, O., Sayer, A. M., Thomas, G. E., McComiskey, A.,
715 Feingold, G., Hoose, C., Kristjánsson, J. E., Liu, X., Balkanski, Y., Donner, L. J., Ginoux,
716 P. A., Stier, P., Grandey, B., Feichter, J., Sednev, Bauer, S. E., Koch, D., Grainger, R. G.,
717 Kirkevåg, A., Iversen, T., Seland, Ø., Easter, R., Ghan, S. J., Rasch, P. J., Morrison, H.,
718 Lamarque, J.-F., Iacono, M. J., Kinne, S., and Schulz, M.: Aerosol indirect effects –
719 general circulation model intercomparison and evaluation with satellite data, *Atmos.*
720 *Chem. Phys.*, 9, 8697–8717, <https://doi.org/10.5194/acp-9-8697-2009>, 2009.
- 721 Randall, D. A., Coakley, J. A., Fairall, C. W., Knopfli, R. A., and Lenschow, D. H.: Outlook
722 for research on marine subtropical stratocumulus clouds. *Bull. Amer. Meteor. Soc.*, 65,
723 1290–1301, 1984.
- 724 Rémillard, J., Kollias, P., Luke, E., and Wood, R.: Marine Boundary Layer Cloud Observations
725 in the Azores, *J. Climate*, 25, 7381–7398, doi: [http://dx.doi.org/10.1175/JCLI-D-11-](http://dx.doi.org/10.1175/JCLI-D-11-00610.1)
726 [00610.1](http://dx.doi.org/10.1175/JCLI-D-11-00610.1), 2012.
- 727 Rémillard, J., Kollias, P., and Szyrmer, W.: Radar-radiometer re- trievals of cloud number
728 concentration and dispersion parameter in nondrizzling marine stratocumulus, *Atmos.*
729 *Meas. Tech.*, 6, 1817–1828, doi:10.5194/amt-6-1817-2013, 2013.
- 730 Slingo, A.: Sensitivity of the Earth’s radiation budget to changes in low clouds, *Nature*, 343,
731 49–51, <https://doi.org/10.1038/343049a0>, 1990.
- 732 Song, H., Zhang, Z., Ma, P.-L., Ghan, S. J., and Wang, M.: An Evaluation of Marine Boundary
733 Layer Cloud Property Simulations in the Community Atmosphere Model Using Satellite
734 Observations: Conventional Subgrid Parameterization versus CLUBB, *J. Clim.*,
735 doi:10.1175/JCLI-D-17-0277.1, 2018.

- 736 Stanfield, R., Dong, X., Xi, B., Gel Genio, A., Minnis, P., and Jiang, J.: Assessment of NASA
737 GISS CMIP5 and post CMIP5 Simulated Clouds and TOA Radiation Budgets Using
738 Satellite Observations: Part I: Cloud Fraction and Properties, *J. Clim.*, doi:10.1175/JCLI-
739 D-13-00588.1, 2014.
- 740 Tripoli, G. J. and Cotton, W. R.: A numerical investigation of several factors contributing to
741 the observed variable intensity of deep convection over South Florida., *J. Appl. Meteorol.*,
742 19, 1037–1063, 1980.
- 743 Troyan, D.: Merged Sounding Value-Added Product, Tech. Rep., DOE/SC-ARM/TR-087,
744 2012.
- 745 Walters, D., Baran, A., Boutle, I., Brooks, M., Earnshaw, P., Edwards, J., Furtado, K., Hill, P.,
746 Lock, A., Manners, J., Morcrette, C., Mulcahy, J., Sanchez, C., Smith, C., Stratton, R.,
747 Tennant, W., Tomassini, L., van Weverberg, K., Vosper, S., Willett, M., Browse, J.,
748 Bushell, A., Dalvi, M., Essery, R., Gedney, N., Hardiman, S., Johnson, B., Johnson, C.,
749 Jones, A., Mann, G., Milton, S., Rumbold, H., Sellar, A., Ujiie, M., Whittall, M., Williams,
750 K. and Zerroukat, M. The Met Office Unified Model Global Atmosphere 7.0/7.1 and
751 JULES Global Land 7.0 configurations. *Geosci. Model Dev.*, doi:10.5194/gmd-2017-291,
752 2017.
- 753 Wang, M., Ghan, S., Liu, X., L'Ecuyer, T. S., Zhang, K., Morrison, H., Ovchinnikov, M.,
754 Easter, R., Marchand, R., Chand, D., Qian, Y., and Penner, J. E.: Constraining cloud
755 lifetime effects of aerosols using A-Train satellite observations, *Geophys. Res. Lett.*, 39,
756 L15709, <https://doi.org/10.1029/2012GL052204>, 2012.
- 757 Warren, S. G., Hahn, C. J., London, J., Chervin, R. M., and Jenne, R.: Global distribution of
758 total cloud cover and cloud type amount over land, Tech. Rep. Tech. Note TN-317 STR,
759 NCAR, 1986.

- 760 Warren, S. G., Hahn, C. J., London, J., Chervin, R. M., and Jenne, R.: Global distribution of
761 total cloud cover and cloud type amount over land, Tech. Rep. Tech. Note TN-317 STR,
762 NCAR, 1988.
- 763 Weber, T., and Quaas, J.: Incorporating the subgrid-scale variability of clouds in the
764 autoconversion parameterization using a PDF-scheme, *J. Adv. Model. Earth Syst.*, 4,
765 M11003, doi:10.1029/2012MS000156, 2012.
- 766 Wielicki, B. A., Cess, R. D., King, M. D., Randall, D. A., and Harrison, E. F.: Mission to planet
767 Earth: Role of clouds and radiation in climate, *Bull. Amer. Meteor. Soc.*, 76, 2125–2153,
768 doi:10.1175/1520-0477(1995)076<2125:MTPERO.2.0.CO;2, 1995.
- 769 Wood, R., Field, P. R., and Cotton, W. R.: Autoconversion rate bias in stratiform boundary
770 layer cloud parameterization. *Atmos. Res.*, 65, 109–128, 2002.
- 771 Wood, R.: Drizzle in stratiform boundary layer clouds. Part I: Vertical and horizontal structure,
772 *J. Atmos. Sci.*, 62, 3011–3033, 2005a.
- 773 Wood, R.: Drizzle in stratiform boundary layer clouds. Part II: Microphysical aspects, *J.*
774 *Atmos. Sci.*, 62, 3034–3050, 2005b.
- 775 Wood, R. and Hartmann, D.: Spatial variability of liquid water path in marine low cloud: The
776 importance of mesoscale cellular convection, *J. Climate*, 19, 1748–1764, 2006.
- 777 Wood, R.: Cancellation of aerosol indirect effects in marine stratocumulus through cloud
778 thinning. *J. Atmos. Sci.*, 64, 2657–2669, 2007.
- 779 Wood, R.: Stratocumulus Clouds, *Mon. Wea. Rev.*, 140, 2373–2423. doi:
780 <http://dx.doi.org/10.1175/MWR-D-11-00121.1>, 2012.
- 781 Wood, R., Wyant, M., Bretherton, C. S., Rémillard, J., Kollias, P., Fletcher, J., Stemmler, J.,
782 deSzoeko, S., Yuter, S., Miller, M., Mechem, D., Tselioudis, G., Chiu, C., Mann, J.,
783 O'Connor, E., Hogan, R., Dong, X., Miller, M., Ghate, V., Jefferson, A., Min, Q., Minnis,
784 P., Palinkonda, R., Albrecht, B., Luke, E., Hannay, C., Lin, Y.: Clouds, Aerosol, and

785 Precipitation in the Marine Boundary Layer: An ARM Mobile Facility Deployment, Bull.
786 Amer. Meteorol. Soc., doi: <http://dx.doi.org/10.1175/BAMS-D-13-00180.1>, 2015.

787 Wu, P., Dong, X. and Xi, B.: Marine boundary layer drizzle properties and their impact on
788 cloud property retrieval, Atmos. Meas. Tech., 8, 3555–3562. doi: 10.5194/amt-8-3555-
789 2015, 2015.

790 Wu, P., Dong, X., Xi, B., Liu, Y., Thieman, M., and Minnis, P.: Effects of environment forcing
791 on marine boundary layer cloud-drizzle processes, J. Geophys. Res. Atmos., 122, 4463–
792 4478, doi:10.1002/2016JD026326, 2017.

793 Xie, X., and Zhang, M.: Scale-aware parameterization of liquid cloud inhomogeneity and its
794 impact on simulated climate in CESM, J. Geophys. Res. Atmos., 120, 8359–8371,
795 doi:10.1002/2015JD023565, 2015.

796 Yoo, H., and Li, Z.: Evaluation of cloud properties in the NOAA/NCEP Global Forecast
797 System using multiple satellite products. Climate Dyn., 39, 2769–2787,
798 doi:10.1007/s00382-012-1430-0, 2012.

799 Yoo, H., and Li, Z., Hou, Y.-T., Lord, S., Weng, F., and Barker, H. W.: Diagnosis and testing
800 of low-level cloud parameterizations for the NCEP/GFS using satellite and ground-based
801 measurements. Climate Dyn., 41, 1595–1613, doi:10.1007/s00382-013-1884-8, 2013.

802 Zhang, J., Lohmann, U., and Lin, B.: A new statistically based autoconversion rate
803 parameterization for use in large-scale models. J. Geophys. Res., 107, 4750,
804 doi:10.1029/2001JD001484, 2002.

805 Zhang, Z., Song, H., Ma, P.-L., Larson, V., Wang, M., Dong, X., and Wang, J.: Subgrid
806 variations of cloud water and droplet number concentration over tropical oceans: satellite
807 observations and implications for warm rain simulation in climate models. Submitted to
808 Atmos. Chem. Phys., 2018.

809

810 **Table 1. The parameters of autoconversion and accretion formulations for four**
 811 **parameterizations.**



812

	A	a_1	a_2	B	b
Khairoutdinov and Kogan (2000)	1350	2.47	-1.79	67	1.15
	$1.3 \times 10\beta_6^6$,				
	where $\beta_6^6 = [(r_v + 3)/r_v]^2$,				
Liu and Daum (2004)	r_v is mean volume radius.	3	-1	N/A	N/A
	modification was made by Wood (2005b)				
Tripoli and Cotton (1980)	3268	7/3	-1/3	1	1
Beheng (1994)	3×10^{34} for $N_c < 200 \text{ cm}^{-3}$ 9.9 for $N_c > 200 \text{ cm}^{-3}$	4.7	-3.3	1	1

813

814 **Table 2. Autoconversion (left) and accretion (right) enhancement factors in different**
 815 **boundary layer conditions (LTS > 18 K for stable, LTS < 13.5 K for unstable and LTS**
 816 **within 13.5 and 18 K for mid-stable) and in different LWP regimes (LWP ≤ 75 g m⁻² for**
 817 **non-precipitating and LWP > 75 g m⁻² for precipitating).**

818

LTS (K)	LWP ≤ 75 g m ⁻²	LWP > 75 g m ⁻²
>18	2.32/1.42	2.75/1.52
 (13.5, 18) 	2.61/1.47	3.07/1.68
<13.5	4.62/1.72	6.94/1.86

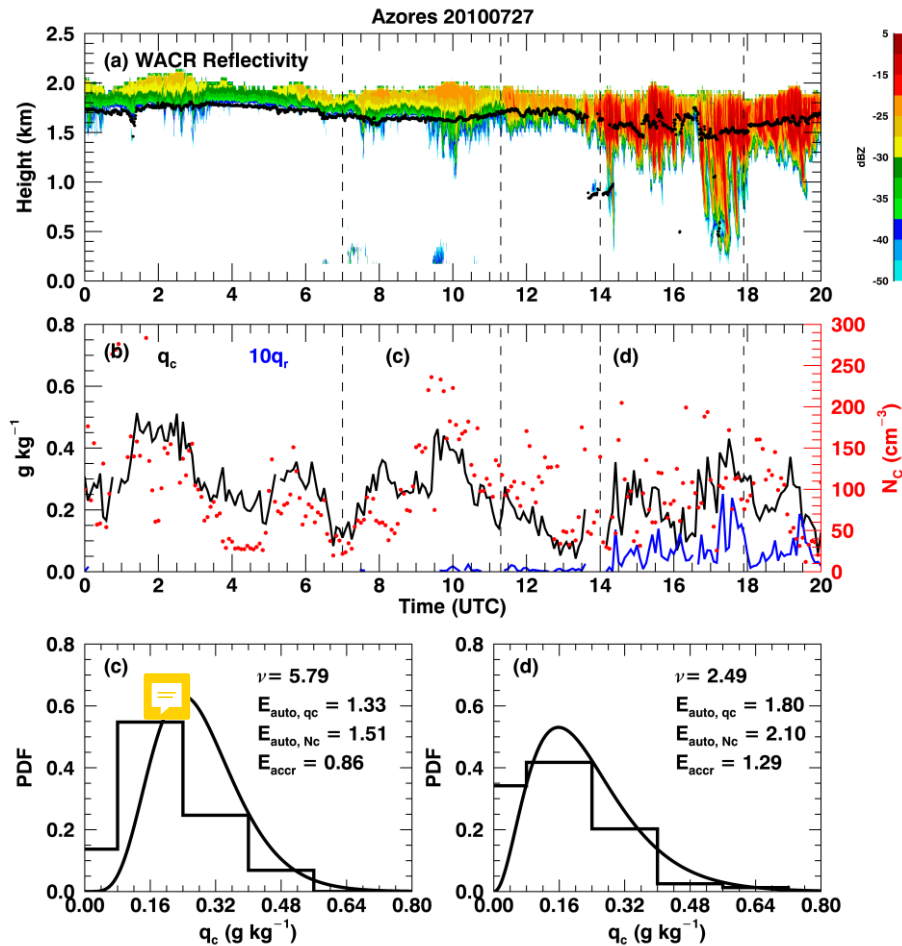
819

820 **Table 3. Autoconversion and accretion enhancement factors (E_{auto} and E_{accr}) for the**
 821 **parameterizations in Table 1 except the Khairoutdinov and Kogan (2000) scheme. The**
 822 **values are averaged for 60-km and 180-km model grids.**

823

	E_{auto}		E_{accr}	
	60-km	180-km	60-km	180-km
Liu and Daum (2004)	3.82	4.23	N/A	N/A
Tripoli and Cotton (1980)	2.46	2.69	1.47	1.56
Beheng (1994)	6.94	5.88	1.47	1.56

824

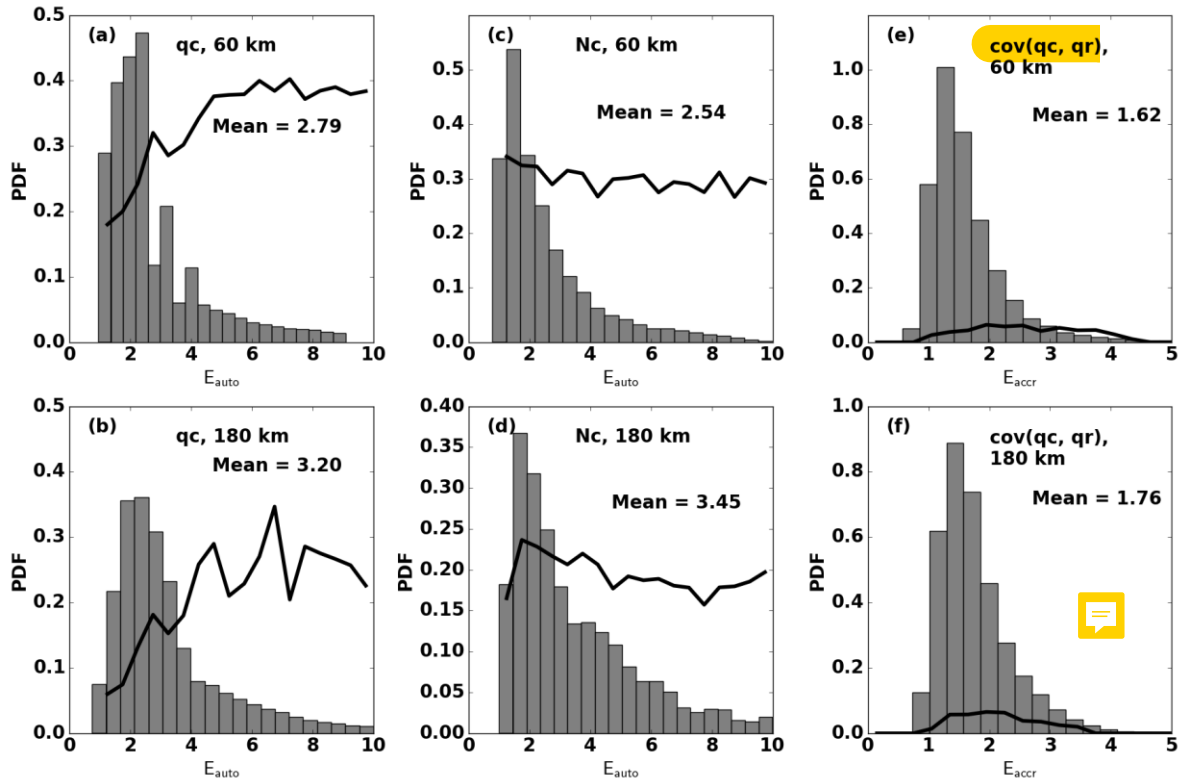


825

826 **Figure 1. Observations and retrievals over Azores on 27 July 2010. (a) W-band ARM**
 827 **cloud radar (WACR) reflectivity (contour) superimposed with cloud-base height (black**
 828 **dots). (b) Black line represents averaged cloud water mixing ratio (q_c) within the top five**
 829 **range gates, blue line represents averaged rain ($\times 10$) water mixing ratio within five range**
 830 **gates around maximum reflectivity, red dots are the retrieved cloud droplet number**
 831 **concentration (N_c). Dashed lines represent two periods that have 60 km model grids with**
 832 **similar mean- q_c but different distributions as shown by step lines in (c) and (d). Curved**
 833 **lines in (c) and (d) are fitted gamma distributions with the corresponding shape**
 834 **parameter (ν) shown on the upper right. N_c distributions are not shown. The calculated**
 835 **autoconversion (E_{auto, q_c} from q_c and E_{auto, N_c} from N_c) and accretion (E_{accr}) enhancement**
 836 **factors are also shown.**

837

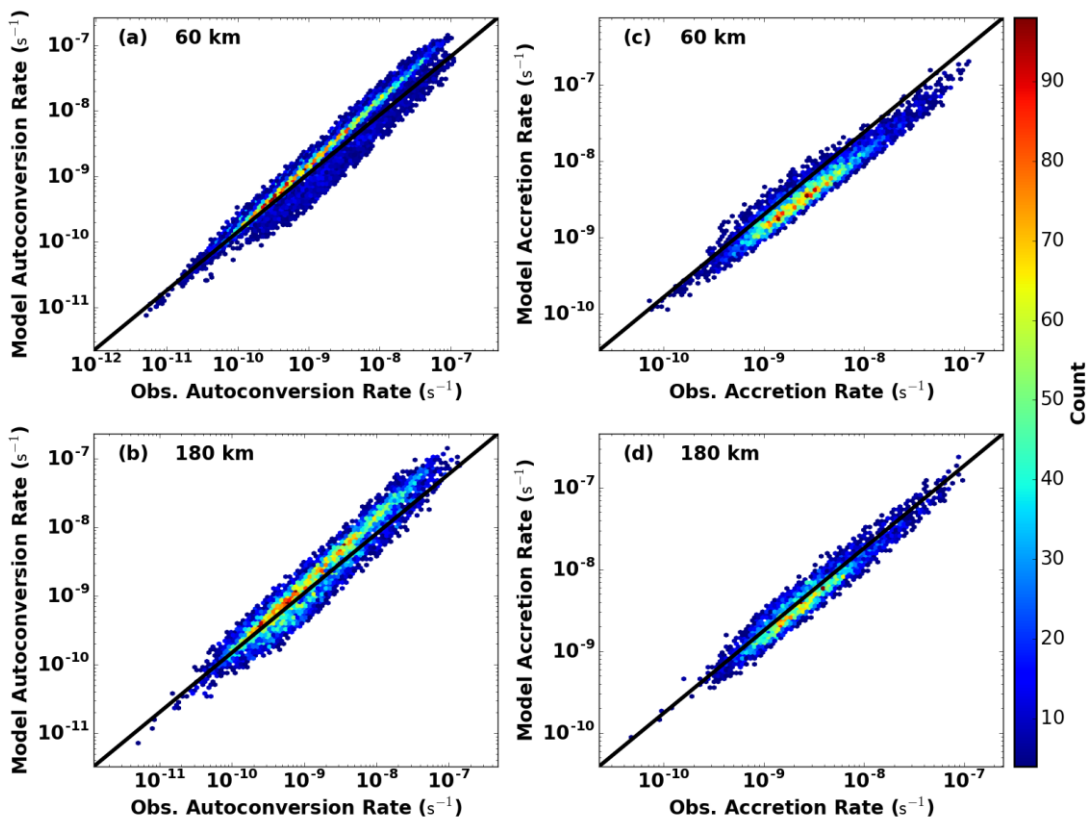
838



839

840 **Figure 2. Probability density functions (PDFs) of autoconversion (a - d) and accretion (e**
 841 **- f) enhancement factors calculated from q_c (a-b), N_c (c-d), and the covariance of q_c and**
 842 **q_r (e-f). The two rows show the results from 60-km and 180-km model grids, respectively,**
 843 **with their average values. Black lines represent precipitation frequency in each bin in (a)-**
 844 **(d) and the ratio of layer-mean q_r to q_c in (e)-(f).**

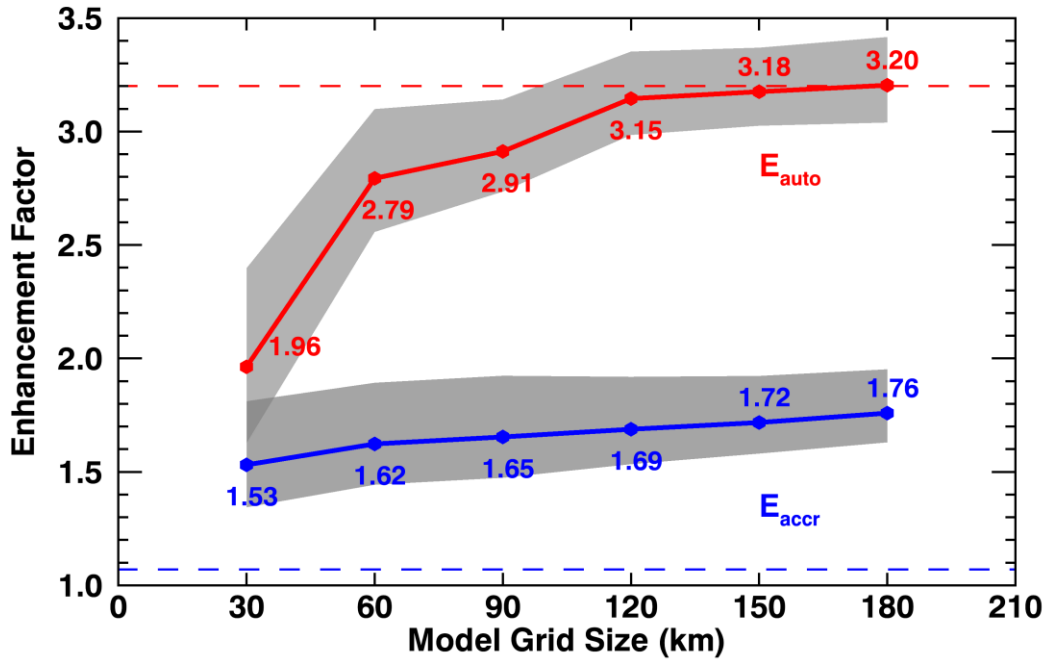
845



846

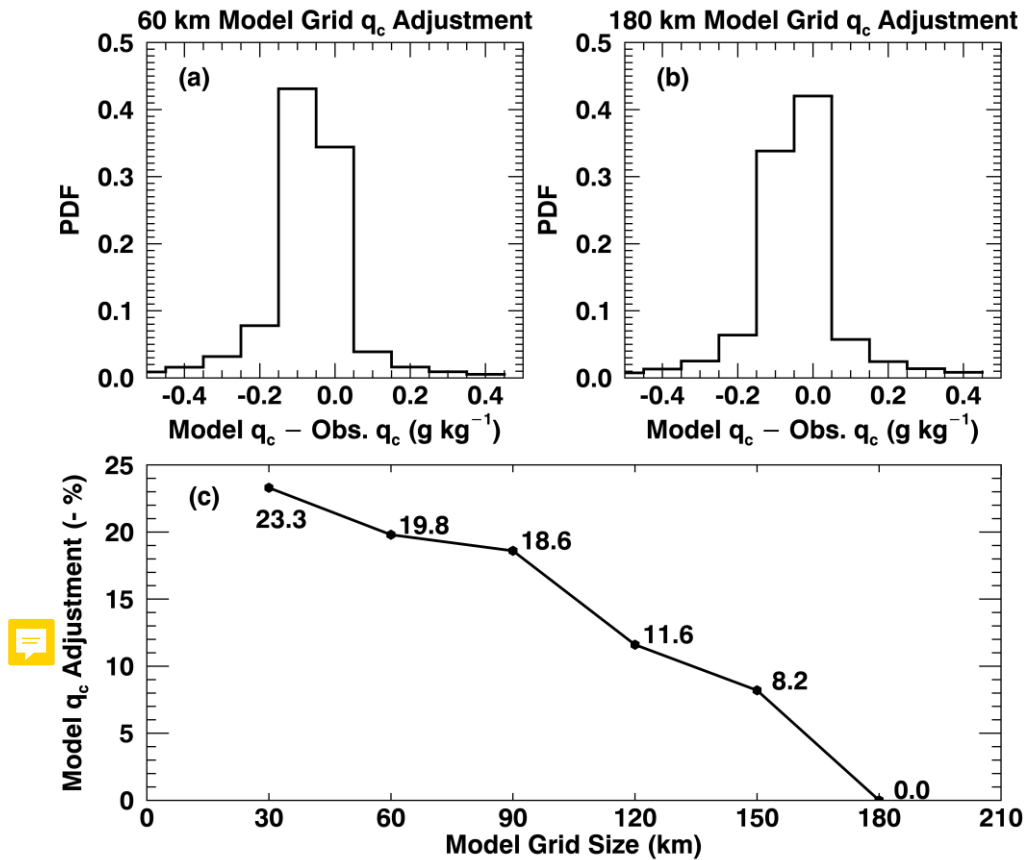
847 **Figure 3.** Comparison of autoconversion (a-b) and accretion (c-d) rates derived from
 848 observations (x-axis) and from model (y-axis). Results are for 60-km (a and c) and 180-
 849 km model grids. Colored dots represent joint number densities.

850



851 **Figure 4. Autoconversion (red line) and accretion (blue line) enhancement factors as a**
 852 **function of model grid sizes. The shaded areas are calculated by varying q_c and q_r within**
 853 **their retrieval uncertainties. The two dashed lines show the constant values of**
 854 **autoconversion (3.2) and accretion (1.07) enhancement factors prescribed in MG08.**

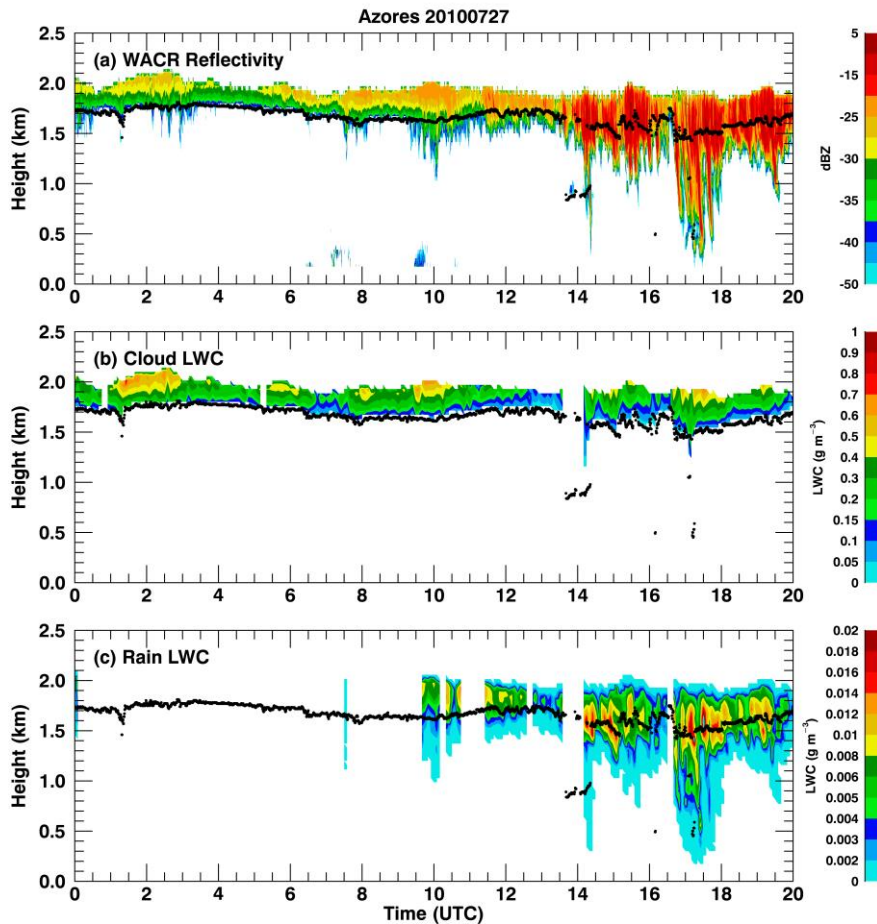
855



856

857 **Figure 5.** q_c needed for models to adjust to reach the same autoconversion rate as
 858 **observations for (a) 60-km and (b) 180-km model grids. Positive biases represent**
 859 **increased q_c are required in models and negative biases mean decreased q_c . The average**
 860 **percentages of adjustments for different model grid sizes are shown in panel (c) and note**
 861 **that the percentages in the vertical axis are negative.**

862



863

864 **Figure A1. Joint retrieval of cloud and rain liquid water content (CLWC and RLWC) for**
 865 **the same case as in Figure 1. (a) WACR reflectivity, (b) CLWC, and (c) RLWC. The black**
 866 **dots represent cloud base height. Blank gaps are due to the data from one or more**
 867 **observations are not available or reliable. For example, the gap before 14 UTC is due to**
 868 **multiple cloud layers are detected whereas we only focus on single layer cloud.**